

4. D. Gabor, Microscopy by reconstructed wavefronts, Proc R Soc A, 197 (1949), 454–487.
5. A. Tennant, G. Junkin, and A.P. Anderson, Advances in phase retrieval metrology, In: 8th International Conference on Antennas and Propagation, ICAP '93, Edinburgh, UK, March 30–April 2, 1993, IEE Conference Publication No. 370, pp. 323–326.
6. S. Costanzo, G.D. Massa, and M.D. Migliore, A novel hybrid approach for far-field characterisation from near-field amplitude-only measurements on arbitrary scanning surfaces, IEEE Trans Antenn Propag 53 (2005), 1866–1873.
7. P. Hariharan, Optical holography, 2nd ed., Cambridge University Press, 1996. ISBN:0–52-131163–2.
8. S. Costanzo, C. Di-Massa, and M.D. Migliore, A X-band probe for phaseless near-field measurements, IEEE Trans Antenn Propag 1 (2002), 274–277.
9. Y.S. El-Said and A.M. Attiya, Modified two probe approach for amplitude only near-field measurements, In: 21st National Radio Science Conference, NRSC 2004, Cairo, Egypt March 16–18, 2004, pp. B2 1–5.
10. D. Smith, M. Leach, and A.J. Sambell, Microwave indirect holographic imaging using an adaptation of optical techniques, IEEE Microwave Wireless Compon Lett 13 (2003), 379–381.
11. D. Smith, M. Leach, M. Elsdon, and S.J. Foti, Imaging of concealed objects from scalar microwave holograms, In: Proceedings of RF and Microwave Conference, Malaysia, Oct. 5–6, 2004, pp. 127–131.
12. E.N. Leith and J. Upatnieks, Wavefront reconstruction and communication theory, J Opt Soc Am 52 (1962), 1123–1130.

© 2006 Wiley Periodicals, Inc.

## INTEGRATION AND INTERPOLATION BASED ON FAST SPHERICAL TRANSFORMS FOR THE MULTILEVEL FAST MULTIPOLE METHOD

Indranil Chowdhury and Vikram Jandhyala

Applied Computational Electromagnetics Laboratory  
Department of Electrical Engineering  
Box 352500  
University of Washington  
Seattle, WA 98195

Received 7 March 2006

**ABSTRACT:** This study presents the application of fast spherical transforms developed by Driscoll and Healy (*Adv Appl Math* 15 (1994), 202–250) to the full-wave multilevel fast multipole method. An accurate uniform-grid based quadrature rule is presented, along with fast algorithms for interpolation and antinterpolation. Error behavior and algorithmic complexities are discussed. Finally an efficient method for the generation of translation operators is presented. The overall method results in efficient and error-controllable schemes for quadrature and interpolation. © 2006 Wiley Periodicals, Inc. *Microwave Opt Technol Lett* 48: 1961–1964, 2006; Published online in Wiley InterScience (www.interscience.wiley.com). DOI 10.1002/mop.21825

**Key words:** multilevel FMM; fast spherical transform; band-limited functions; interpolation and antinterpolation

### 1. INTRODUCTION

The multilevel fast multipole method (MLFMM) [1, 2] is used in integral equation methods to accelerate the  $O(N^2)$  direct matrix–vector product to an  $O(N \log N)$  process. The full-wave MLFMM has been used to solve equivalent dense matrix systems resulting from the Method of Moments with large number of unknowns, which were previously computationally unfeasible [3]. It has been

applied to surface integral equations [4, 5] and volume integral equations [6] for scattering problems.

The MLFMM algorithm consists of two sweeps. In the first sweep, outgoing plane-wave expansions due to  $N$  basis functions are constructed at the finest level. These expansions are then interpolated and combined to form outgoing plane-wave expansions at higher levels. In the second sweep, the outgoing plane waves are translated into local incoming plane waves, which are then antinterpolated and shifted to incoming plane wave expansions at lower levels. At the finest level, the incoming waves are reconstituted via spectral integration to give the fields at the  $N$  testing functions. Key issues in MLFMM are the control of errors arising in the spectral integration, interpolation, and the antinterpolation steps.

Until recently, interpolation and antinterpolation were performed by Lagrangian polynomial technique and other schemes based on approximate prolate spheroid series (APS) and Tschebysheff sampling (TS) [2, 7]. Recently, another efficient scheme for interpolation and antinterpolation based on FFTs was developed [8]. Present methods for numerical quadrature over the unit sphere rely on Gaussian quadrature in the elevation ( $\theta$ ) direction and trapezoidal rule in the azimuthal ( $\varphi$ ) direction [2]. Such quadrature schemes are efficient for band-limited functions, but they use nonuniform grids, over which interpolation becomes expensive. Interpolation schemes based on uniform grids (APS and TS) are fast, but are not suitable for accurate quadrature [9].

This study proposes an accurate, uniform grid-based quadrature scheme using band-limited functions on the 2-sphere ( $S^2$ ), which were introduced by Driscoll and Healy [10]. Fast and accurate interpolation of plane-wave expansions are implemented using fast spherical transforms developed earlier [10, 11]. These transforms are also used for the generation of the translation operator efficiently.

### 2. BAND-LIMITED FUNCTIONS ON $S^2$

The Fourier expansion of a function  $f$  on the 2-sphere is defined as,

$$f = \sum_{l \in \mathbb{Z}} \sum_{|m| \leq l} \hat{f}(l, m) Y_l^m \quad (1)$$

The function  $f$  is called a band-limited function if  $\hat{f}(l, m) = 0, \forall l \geq b$ , where  $b$  is the band-limit.  $Y_l^m$  is the normalized spherical harmonic of degree  $l$  and order  $m$ . The Fourier coefficients are given by,

$$\hat{f}(l, m) = \int_{S^2} d^2\hat{\mathbf{k}} f(\hat{\mathbf{k}}) Y_l^{-m}(\hat{\mathbf{k}}) \quad (2)$$

A sampling theorem for band-limited functions proved by Driscoll and Healy [10] states that,

$$\hat{f}(l, m) = \frac{\sqrt{2\pi}}{2b} \sum_{j=0}^{2b-1} \sum_{k=0}^{2b-1} a_{j+1/2}^{(2b)} f(\theta_j, \phi_k) Y_l^{-m}(\theta_j, \phi_k), \quad (3)$$

where,  $\theta_k$  and  $\phi_k$  are the Chebyshev nodes given by  $\theta_j = (2j + 1)\pi/4b$ ,  $\phi_k = \pi k/b$ , and the weights  $a_j^{(2b)}$  are given by,

$$a_j^{(n)} = \frac{2\sqrt{2}}{n} \sin\left(\frac{\pi j}{n}\right) \sum_{l=0}^{n/2-1} \frac{1}{2l+1} \sin(2l+1)\frac{\pi j}{n}, \quad j = 0, 1, \dots, n-1. \quad (4)$$

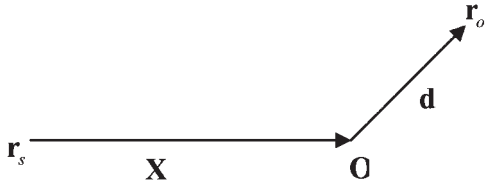


Figure 1 Location of source and observer points

This theorem [Eq. (3)] is *exact* for band-limited functions. There are  $b^2$  coefficients in Eqs. (1) and (3) requires  $4b^2$  samples for computation of each of these coefficients. Thus, the forward transform requires  $4b^4$  operations. Similarly, the inverse transform for recovering the  $4b^2$  samples given the  $b^2$  Fourier coefficients also requires  $4b^4$  operations. In the earlier works [10, 11], both the forward and inverse transforms are accelerated by using  $O(N_s \log^2 N_s)$  algorithms, where  $N_s$  is the number of samples. These algorithms combine the fast Legendre transform over the  $\theta$  direction and the FFT over the  $\phi$  direction. An implementation of the ideas [11] can be found online, in the software package **S2kit** at <http://www.cs.dartmouth.edu/>. The next section will demonstrate that these ideas can be applied to the accurate and efficient computation of the operators in full-wave FMM.

### 3. APPLICATION IN FULL-WAVE MLFMM

This section deals with the following FMM steps: quadrature, interpolation, anterpolation, and computation of the diagonal translation operators.

#### 3.1 Quadrature Over Unit Sphere

Consider a field point  $\mathbf{r}_o$  and a source point  $\mathbf{r}_s$  (Fig. 1). Then, the vector separating these two points is given by  $\mathbf{r}_o - \mathbf{r}_s = \mathbf{X} + \mathbf{d}$ . Let,  $d = |\mathbf{d}|$  and  $X = |\mathbf{X}|$ , then, the Green's function is given by,

$$\frac{e^{ik|\mathbf{X}+\mathbf{d}|}}{|\mathbf{X} + \mathbf{d}|} = ik \sum_{l=0}^{\infty} (-1)^l (2l+1) j_l(kd) h_l^{(1)}(kX) P_l(\hat{\mathbf{d}} \cdot \hat{\mathbf{X}}), \quad (5)$$

$$= \frac{ik}{4\pi} \int d^2 \hat{\mathbf{k}} e^{ikd} T_L(\mathbf{X}, \mathbf{k}) + \varepsilon_T, \quad (6)$$

where  $\varepsilon_T$  is the error due to the truncation of the infinite series in Eq. (5), and  $T_L$  is the truncated translation operator given by,

$$T_L(\mathbf{r}, \mathbf{k}) = \sum_{l=0}^{L-1} i^l (2l+1) h_l^{(1)}(kr) P_l(\hat{\mathbf{r}} \cdot \hat{\mathbf{k}}) = \sum_{l=0}^{L-1} \sum_{m=-l}^l i^l (2l+1) h_l^{(1)} \times (kr) Y_l^m(\hat{\mathbf{r}}) Y_l^{-m}(\hat{\mathbf{k}}). \quad (7)$$

Bounding values of  $\varepsilon_T$  can be found in Ref. [9]. Comparing Eqs. (5), (6), and (2), each term inside the summation is a Fourier coefficient of an expansion over the unit sphere. As a result, the sampling theorem can be applied and [Eq. (5)] can be written as,

$$\frac{e^{ik|\mathbf{X}+\mathbf{d}|}}{|\mathbf{X} + \mathbf{d}|} = \frac{ik\sqrt{2}}{4L} \sum_{p=0}^{2L-1} \sum_{q=0}^{2L-1} a_{p+1/2}^{(2L)} e^{ik_{pq}d} T_L(\mathbf{X}, \mathbf{k}_{pq}) + \varepsilon_l + \varepsilon_T, \quad (8)$$

where  $\varepsilon_l$  is the error incurred while replacing the integration by weighted summation over the  $4L^2$  samples. To get an expression for  $\varepsilon_l$ , consider the Fourier expansion,

$$e^{ikd} = \sum_{\nu=0}^{\infty} i^\nu (2\nu+1) j_\nu(kd) P_\nu(\hat{\mathbf{k}} \cdot \hat{\mathbf{d}}). \quad (9)$$

Therefore the integral in Eq. (6) can be written as,

$$\frac{ik}{4\pi} \int d^2 \hat{\mathbf{k}} \sum_{\nu=0}^{L-1} i^\nu (2\nu+1) j_\nu(kd) P_\nu(\hat{\mathbf{k}} \cdot \hat{\mathbf{d}}) T_L(\mathbf{X}, \mathbf{k}) + \frac{ik}{4\pi} \int d^2 \hat{\mathbf{k}} \sum_{\nu=L}^{\infty} i^\nu (2\nu+1) j_\nu(kd) P_\nu(\hat{\mathbf{k}} \cdot \hat{\mathbf{d}}) T_L(\mathbf{X}, \mathbf{k}). \quad (10)$$

By orthogonality of the spherical harmonics, the second term is zero. This is because all the spherical harmonics in  $T_L$  are of order  $\nu < L$ , while the spherical harmonics in  $P_\nu(\hat{\mathbf{k}} \cdot \hat{\mathbf{d}})$  are of order  $\nu \geq L$ . The first term is exactly

$$\frac{ik\sqrt{2}}{4L} \sum_{p=0}^{2L-1} \sum_{q=0}^{2L-1} a_{p+1/2}^{(2L)} T_L(\mathbf{X}, \mathbf{k}_{pq}) \times \left[ \sum_{\nu=0}^{L-1} i^\nu (2\nu+1) j_\nu(kd) P_\nu(\hat{\mathbf{k}}_{pq} \cdot \hat{\mathbf{d}}) \right]. \quad (11)$$

Thus, the error  $\varepsilon_l$  is given by,

$$\begin{aligned} \varepsilon_l &= -\frac{ik\sqrt{2}}{4L} \sum_{p=0}^{2L-1} \sum_{q=0}^{2L-1} a_{p+1/2}^{(2L)} [e^{ik_{pq}d} T_L(\mathbf{X}, \mathbf{k}_{pq}) \\ &\quad - \sum_{\nu=0}^{L-1} i^\nu (2\nu+1) j_\nu(kd) P_\nu(\hat{\mathbf{k}}_{pq} \cdot \hat{\mathbf{d}}) T_L(\mathbf{X}, \mathbf{k}_{pq})] \\ &= -\frac{ik\sqrt{2}}{4L} \sum_{p=0}^{2L-1} \sum_{q=0}^{2L-1} a_{p+1/2}^{(2L)} \\ &\quad \times \left[ \sum_{\nu \geq L} i^\nu (2\nu+1) j_\nu(kd) P_\nu(\hat{\mathbf{k}}_{pq} \cdot \hat{\mathbf{d}}) T_L(\mathbf{X}, \mathbf{k}_{pq}) \right]. \end{aligned} \quad (12)$$

This error decreases exponentially with increasing  $L$ , since  $j_\nu(kd)$  decreases exponentially for  $\nu > kd$ . Typically,  $L$  is chosen according to the formula [9]:

$$L = kd + C_\alpha (kd)^{1/3}, \quad (13)$$

where,  $C_\alpha$  is a parameter chosen to control the accuracy of the calculations. This error is nonzero because the quadrature rule [Eq. (8)] is constructed using samples of the plane wave function  $e^{i\mathbf{k} \cdot \mathbf{d}}$ , which, from Eq. (9), is not exactly band-limited. Hence, the quadrature error  $\varepsilon_l$  can also be interpreted as an *aliasing* error, which arises due to the presence of spherical harmonics of degree  $\nu \geq L$ , in the plane wave function.

Figure 2 plots the relative errors using the truncated series [Eq. (5)], and the quadrature rules [Eqs. (8) and (11)]. The relative error is defined according by

$$E = \frac{\|G(X, d) - \tilde{G}(X, d)\|}{\|G(X, d)\|}, \quad (14)$$

where,  $G(X, d)$  is the free-space Green's function  $\frac{e^{ik|\mathbf{X}+\mathbf{d}|}}{|\mathbf{X} + \mathbf{d}|}$ , and  $\tilde{G}(X, d)$  represents one of Eqs. (5), (8) and (11). From the plot, it can be seen that the truncated series in Eq. (5) coincides with Eq. (11). The quadrature rule [Eq. (8)] contains the extra aliasing error

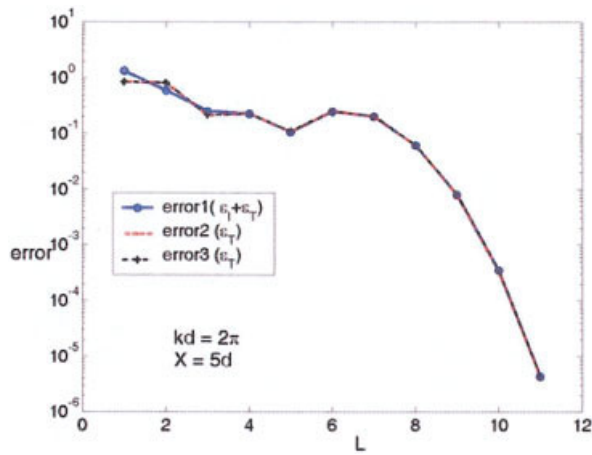


**Figure 2** Comparison of errors due to quadrature rules: error1 (3.4), error2 (3.7) and error3 (3.1). [Color figure can be viewed in the online issue, which is available at [www.interscience.wiley.com](http://www.interscience.wiley.com)]

$\varepsilon_T$ . For lower values of  $L$ ,  $\varepsilon_T$  and  $\varepsilon_I$  are comparable. As  $L$  increases  $\varepsilon_T$  begins to dominate, making the total error bounded by  $\varepsilon_T$ . This has also been pointed out in Ref. [9]. The quadrature rule [Eq. (8)] is optimal, since the leading error is incurred during truncation.

Quadrature of band-limited functions can be performed accurately by using Gaussian quadrature in the  $\theta$  direction and trapezoidal rule in the  $\phi$  direction [1, 2, 9]. However, this kind of a scheme uses a nonuniform grid, over which performing interpolation becomes costly. The advantage of the quadrature rule presented in this study is the use of uniform grid in both the directions, making interpolation by means of a 2-D FFT directly applicable. In the next subsection, accurate and efficient interpolation schemes using fast spherical transforms will be discussed.

### 3.2 Interpolation and Anterpolation Using Spherical Transforms

The radiation pattern  $f(\theta, \phi)$  at a particular level can be approximately represented by the band-limited Fourier expansion,

$$f(\theta, \phi) \approx \sum_{l=0}^{L-1} \sum_m -1l \hat{f}(l, m) Y_l^m(\theta, \phi), \quad (15)$$

where,  $L$  is the bandwidth chosen at that level. Note that, at any level  $L$  is infinity for the expansion (15) to be exact. In practice, only a finite number of samples (in this case  $4L^2$ , evaluated at the Chebyshev nodes, are stored at each level. During interpolation to a new bandwidth  $L' > L$ , two steps are required:

- i. FST ( $f_L \rightarrow \hat{f}_L$ ): The forward spherical transform (FST) step, which involves computation of the  $L^2$  Fourier coefficients in (13) from the  $4L^2$  samples. This is accomplished in  $O(16L^2 \log^2 L)$  operations using the fast forward spherical transform algorithm [11].
- ii. IST ( $\hat{f}_L \rightarrow f_{L'}$ ): The inverse spherical transform (IST) step, which evaluates the  $4L'^2$  samples at the new bandwidth from the  $L^2$  Fourier coefficients. Using the fast inverse transform algorithm, this step requires  $O(16L'^2 \log^2 L')$  operations [11]. Thus, the interpolation step has a complexity of  $O(16L'^2 \log^2 L') + O(16L^2 \log^2 L)$ . The interpolation scheme is not exact, because from Eq. (9)  $f$  is not exactly band-limited. However, this error can be kept low by choosing  $L > kd$ . Also, the leading error is incurred during truncation and not during interpolation. The interpolation error does not grow with increasing harmonic

content, since at higher levels proportionately more samples are used. Anterpolation consists of the same two steps of forward and inverse transforms. Examples of the error behavior during interpolation and anterpolation are shown in Figure 3.

In the existing methods [1, 2, 9], the Gaussian quadrature schemes use nonuniform grids, while uniform grids are used in schemes based on prolate spheroid or Chebyshev sampling series [7]. In the latter scheme, quadrature is not as accurate as the Gauss-Legendre scheme. On the other hand, Gauss-Legendre quadrature is more accurate, but Lagrangian interpolation schemes need to be used to perform accurate interpolation on nonuniform grids, thereby increasing the cost. The scheme presented herein simultaneously offers accurate quadrature [Eq. (8)] as well as efficient interpolation (15). Also, it does not require the function to be over-sampled as in the case of the APS method. However, the total matrix-vector product becomes  $O(N \log^2 N)$ , because the interpolation cost at each level is  $O(L^2 \log^2 L)$ .

### 3.3 Computation of Translation Operator

The computation of the translation operator [Eq. (7)] requires  $L$  operations in each of the  $4L$  [1] directions, making the total cost  $4L^3$ . This makes the setup of the translation operators for large values of  $L$  very expensive. This problem has been addressed in [2, 12] by sampling the function  $T_L$  at  $O(L)$  sample points and then performing an  $O(L^2)$  interpolation to obtain the values at the required directions. Although this brings down the complexity, an error is introduced in the process of interpolation. The computation of the translation operator can be expedited, as well as made exact, by noting that by the definition (1), Eq. (7) is a Fourier expansion of order  $L$  with coefficients,

$$\hat{f}(l, m) = i^{l(2l+1)} h_l^{(1)}(kr) Y_l^m(\hat{\mathbf{r}}). \quad (16)$$

This makes the fast inverse transform directly applicable. The steps of computing the translation operator  $T_L(\mathbf{r}, \mathbf{k})$  are therefore,

- i. Compute the  $L^2$  Fourier coefficients of the band-limited expansion  $T_L(\mathbf{r}, \mathbf{k})$  [Eq. (7)], using Eq. (16). This step requires  $O(L^2)$  operations.
- ii. Using the fast inverse transform, compute the  $4L'^2$  values of  $T_{L'}(\mathbf{r}, \mathbf{k})$  at the Chebyshev sampling nodes. This step requires  $O(16L'^2 \log^2 L')$  operations.

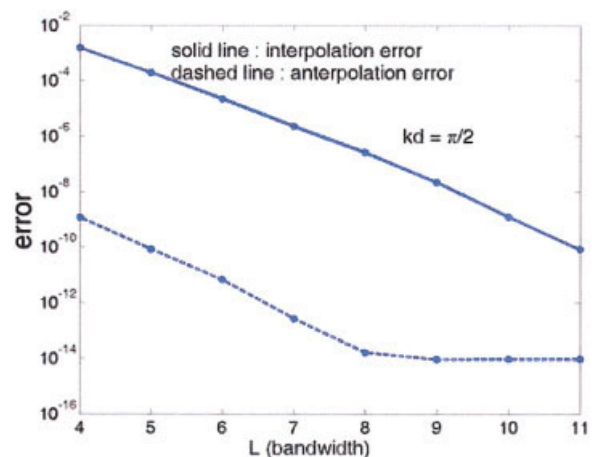


**Figure 3** Error incurred in interpolation and anterpolation from  $L$  to  $2L$ . [Color figure can be viewed in the online issue, which is available at [www.interscience.wiley.com](http://www.interscience.wiley.com)]

Thus total cost of the setup of translation operators is  $O(16L^2 \log^2 L + L^2)$ . This is an exact and fast method to compute Eq. (7). Hence, the fast spherical transforms are useful in the setup of the translation operators in addition to quadrature and interpolation.

#### 4. CONCLUSION

In this study, the fast spherical transforms were applied to the full-wave MLFMM in order to propose efficient and error-controllable quadrature, interpolation, and anterpolation schemes, along with fast generation of translation operators. None of the FMM operations in this paper uses approximating polynomials like Lagrangian polynomials or the prolate spheroid series, and are completely based on spherical harmonics that are inherently present in the kernel under consideration. The only disadvantage of the presented method is that its overall cost is  $O(N \log^2 N)$ , as opposed to the  $O(N \log N)$  algorithm based on the APS method.

#### REFERENCES

1. R. Coifman, V. Rokhlin, and S. Wandzura, The fast multipole method for the wave equation: A pedestrian prescription, *IEEE Antennas Propagat Mag* 35 (1993), 7–12.
2. W.C. Chew, J.-M. Jin, E. Michielssen, J. Song, Fast and efficient algorithms in computational electromagnetics, Artech House Inc., Norwood, 2001.
3. S. Valampambal, W.C. Chew, and J.M. Song, 10 million unknowns, Is that big? *IEEE Antennas Propagat Mag* 45 (2003), 45–58.
4. J.M. Song and W.C. Chew, Multilevel fast multipole algorithm for solving CFIE of electromagnetic scattering, *Microwave Opt Tech Lett* 10 (1995), 14–19.
5. J.M. Song, C.C. Lu, and W.C. Chew, Multilevel fast multipole algorithm for electromagnetic scattering by large complex objects, *IEEE Trans Antennas Propagat* 45 (1997), 1488–1493.
6. K. Sertel and J. Volakis, Multilevel fast multipole solution of volume integral equations using parametric geometry modeling, *IEEE Trans Antennas Propagat* 52 (2004), 1686–1692.
7. O.M. Bucci and C. Gennareli, Fast and accurate near-field-far-field transformation by sampling interpolation of polar measurements, *IEEE Trans Antennas Propagat* 39 (1991), 48–55.
8. J. Sarvas, Performing interpolation and anterpolation entirely by FFT in the 3-D multilevel fast multipole algorithm, *SIAM J Numerical Anal* 41 (2003), 2180–2196.
9. S. Koc, J. Song, and W.C. Chew, Error analysis for the numerical evaluation of the diagonal forms of the scalar spherical addition theorem. *SIAM J Numerical Anal* 36 (1999), 906–921.
10. J.R. Driscoll and D.M. Healy, Computing Fourier transforms and convolutions on the 2- Sphere, *Adv Appl Math* 15 (1994), 202–250.
11. D. Healy, Jr., D. Rockmore, P. Kostelec, and S. Moore, FFTs for the 2-sphere—improvements and variations, *J Fourier Anal Appl* 9 (2003), 341–385.
12. J. Song, W.C. Chew, Interpolation of translation matrix in MLFMA, *Microwave Opt Tech Lett* 30 (2001), 109–114.

© 2006 Wiley Periodicals, Inc.

## HIGH SELECTIVE STEPPED-IMPEDANCE DUAL-BAND BANDPASS FILTER

Jianpeng Wang,<sup>1,2</sup> Yong-Xin Guo,<sup>1</sup> Bing-Zhong Wang,<sup>2</sup> and L. C. Ong<sup>1</sup>

<sup>1</sup> Institute for Infocomm Research, Singapore 117674

<sup>2</sup> Institute of Applied Physics, University of Electronic Science and Technology of China, Chengdu, China

Received 5 March 2006

**ABSTRACT:** A high selective stepped-impedance dual-band bandpass filter is presented. The filter has a feature of two tunable passbands over a wide frequency range and compact size. A multi-coupling scheme is introduced so that two finite transmission zeros are generated between the two passbands to achieve a high out-of-band rejection. © 2006 Wiley Periodicals, Inc. *Microwave Opt Technol Lett* 48: 1964–1966, 2006; Published online in Wiley InterScience (www.interscience.wiley.com). DOI 10.1002/mop.21831

**Key words:** dual-band bandpass filters; stepped impedance resonator; transmission zeros; wireless local area network (LAN)

#### 1. INTRODUCTION

The increasing demand of wireless communication applications necessitates RF transceivers operating in multiple separated frequency bands so that users can access various services with a single multimode handset or terminal. For example, Global systems for mobile communications (GSMs) operate at both 900 and 1800 MHz, IEEE 802.11b and IEEE 802.11a wireless local area network (LAN) products operate in the unlicensed industrial–scientific–medical (ISM) 2.4 GHz band and 5 GHz, respectively. Therefore, dual-band filters have recently received much attention [1–5]. Compact size, high performance, and low cost are the requirements for the dual-band bandpass filter designs. With the LTCC technique [1], a dual-band filter for multimode GSM was designed using two stacked single-band bandpass filters. By incorporating step-impedance resonators in a comb-filter topology, a dual-band bandpass filter with one transmission zero between the two pass bands was designed [2], in which the two pass bands are generated by the parallel coupling section of resonators. Dual-band bandpass filters in parallel-coupled and vertical-stacked configurations were proposed in Ref. 3. On the basis of the resonance characteristics of a stepped impedance resonator (SIR), the second resonant frequency in Refs. 2 and 3 can be tuned over a wide range by adjusting its structure parameters. However, the insertion loss in the pass band may increase because of the multilevel stepped impedance resonator coupling. Using equal-length coupled-serial-shunted lines and z-transform technique, a high performance dual-band filter was designed although the filter size is increased [4]. To reduce the overall electrical length and realize cross coupling a tri-section stepped-impedance resonator for bandpass filters design was introduced in Ref. 5.

In this article, a new configuration of a dual-band filter is presented. Two pass bands located at the desired frequencies are realized through adjusting the structure parameters of the SIR. A multicoupling scheme is introduced on the filter design so that two finite transmission zeros are generated between the two pass bands. A high-selective dual pass band filter is obtained with a simple structure and a compact size. As one example, one dual-band filter for wireless LAN applications is designed.